

# Discovery of Potent and Selective Inhibitors of Wild-Type and Gatekeeper Mutant Fibroblast Growth Factor Receptor (FGFR) 2/3

Artem Shvartsbart,\* Jeremy J. Roach, Michael R. Witten, Holly Koblish, Jennifer J. Harris, Maryanne Covington, Rodrigo Hess, Luping Lin, Michelle Frascella, Lisa Truong, Lynn Leffet, Patricia Conlen, Elham Beshad, Ron Klabe, Kamna Katiyar, Laura Kaldon, Ruth Young-Sciame, Xin He, Susan Petusky, Kwang-Jong Chen, April Horsey, Hsiang-Ting Lei, Leslie B. Epling, Marc C. Deller, Oleg Vechorkin, and Wenqing Yao



Cite This: *J. Med. Chem.* 2022, 65, 15433–15442



Read Online

ACCESS |



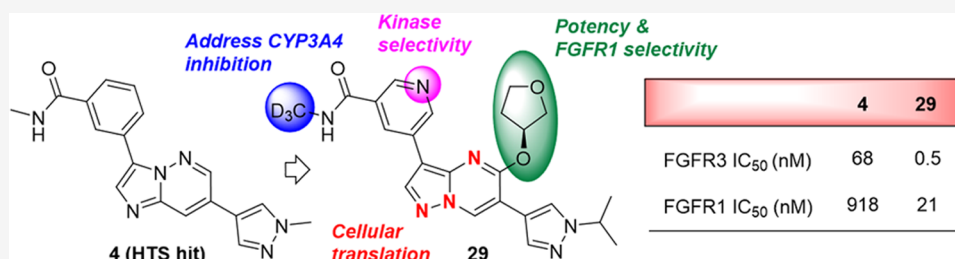
Metrics & More



Article Recommendations



Supporting Information



**ABSTRACT:** Upregulation of the fibroblast growth factor receptor (FGFR) signaling pathway has been implicated in multiple cancer types, including cholangiocarcinoma and bladder cancer. Consequently, small molecule inhibition of FGFR has emerged as a promising therapy for patients suffering from these diseases. First-generation pan-FGFR inhibitors, while highly effective, suffer from several drawbacks. These include treatment-related hyperphosphatemia and significant loss of potency for the mutant kinases. Herein, we present the discovery and optimization of novel FGFR2/3 inhibitors that largely maintain potency for the common gatekeeper mutants and have excellent selectivity over FGFR1. A combination of meticulous structure–activity relationship (SAR) analysis, structure-based drug design, and medicinal chemistry rationale ultimately led to compound **29**, a potent and selective FGFR2/3 inhibitor with excellent *in vitro* absorption, distribution, metabolism, excretion (ADME), and pharmacokinetics in rat. A pharmacodynamic study of a closely related compound established that maximum inhibition of downstream ERK phosphorylation could be achieved with no significant effect on serum phosphate levels relative to vehicle.

## INTRODUCTION

Fibroblast growth factor receptors (FGFR1–4) are a family of transmembrane receptor tyrosine kinases that play a role in several physiological processes, including embryonic development, metabolic homeostasis, and angiogenesis.<sup>1</sup> Aberrant activation of FGFR signaling leads to proliferation and survival of cancer cells, with FGFR3 alterations most commonly found in bladder cancer,<sup>2</sup> while FGFR2 alterations are mainly found in cholangiocarcinoma, gastric cancer, and uterine cancer.<sup>2–4</sup> Three ATP-competitive small molecule pan-FGFR (FGFR1–3) inhibitors have been approved by the FDA for the treatment of cancers with FGFR genetic alterations (Figure 1). Erdafitinib<sup>5–7</sup> (**1**) was approved to treat locally advanced or metastatic urothelial carcinoma (bearing FGFR3 or FGFR2 genetic alteration), while pemigatinib<sup>8,9</sup> (**2**) and infigratinib<sup>10</sup> (**3**) were approved to treat locally advanced or metastatic cholangiocarcinoma (bearing FGFR2 alteration). The most common treatment-related toxicity for these drugs is hyperphosphatemia. Since antibody-mediated FGFR1 activation in

mice leads to hypophosphatemia, while FGFR1/4 knockout mice experienced hyperphosphatemia, this toxicity has been hypothesized to be due to FGFR1 inhibition.<sup>11,12</sup>

Inhibitors **1–3** derive a large amount of binding energy from an optionally substituted 3,5-dimethoxyphenyl group that projects past the gatekeeper (GK) residue into a hydrophobic pocket. Clinical resistance to currently approved FGFR inhibitors has been reported and results predominantly from GK mutations (FGFR2 V564I/L/M/F, FGFR3 V555I/L/M/F).<sup>13,14</sup> The GK residue in each mutant is larger than the valine of the wild-type kinase and can no longer accommodate the 3,5-dimethoxyphenyl group of **1–3**.

**Received:** August 18, 2022

**Published:** November 10, 2022



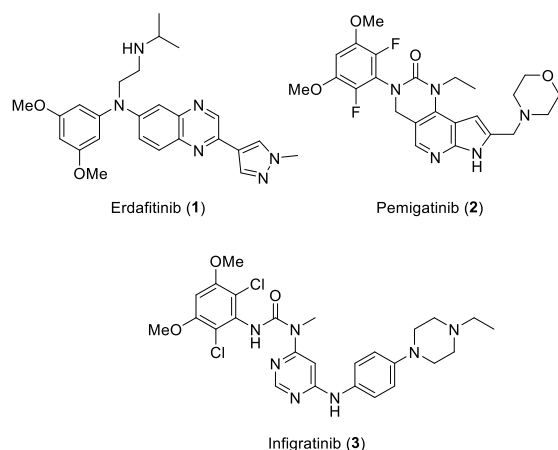


**Figure 1.** FDA-approved pan-FGFR (FGFR1–3) inhibitors erdafitinib, pemigatinib, and infigratinib.

Consequently, an FGFR inhibitor of an alternative chemotype that does not rely on this interaction for potency is highly desirable. Based on these data, we sought to develop a second-generation FGFR3 inhibitor with equal potency for the wild-type kinase and gatekeeper mutants, >20-fold selectivity over FGFR1, and a pharmacokinetic profile suitable for oral dosing. Equal potency for FGFR2 was also desirable, though not a formal goal. Therefore, FGFR3 enzymatic and cellular screening was used to drive the SAR discussed herein.

## RESULTS AND DISCUSSION

Our program was initiated with a high-throughput screening (HTS) campaign, which identified several potential scaffolds. One of these was an imidazo[1,2-*b*]pyridazine series, from which **4** was discovered (Table 1). Compound **4** had good

**Table 1.** HTS Hit **4** and Methoxy Derivative **5**

compd	R <sup>1</sup>	FGFR3 IC <sub>50</sub> (nM)	FGFR3 V555L IC <sub>50</sub> (nM)	FGFR1 IC <sub>50</sub> (nM)
<b>4</b>	H	68	22	918
<b>5</b>	OMe	4.6		86

potency for FGFR3 WT (IC<sub>50</sub> = 68 nM) and GK mutant FGFR3 V555L (IC<sub>50</sub> = 22 nM), with >10-fold selectivity over FGFR1, providing an excellent starting point for our discovery campaign.

The *N*-methyl amide proved to be a key component of the pharmacophore. Analysis of related HTS hits revealed that compounds without this precise substituent were significantly less potent and selective. We briefly examined other modifications to the amide or replacement with isosteres, but there was no improvement over **4** (data not shown). Given the very high structural homology between FGFR3 and FGFR1, molecular modeling was unsuccessful in explaining the selectivity imparted by the amide. One possible explanation is a subtle conformational change in the P-loop between these two isoforms.

Substitution on the carbon adjacent to the pyridazine nitrogen (R<sup>1</sup>) was subsequently explored. We quickly identified methoxy derivative **5** (Table 1), which had an improved potency in FGFR3 (IC<sub>50</sub> = 4.6 nM) while maintaining similar levels of selectivity over FGFR1 (19×) compared to **4**.

Replacement of the phenyl ring of **5** with *m*-pyridyl was tolerated, as exemplified by **6** (Table 2). The ensuing SAR was

**Table 2.** SAR Adjacent to the Pyridazine Nitrogen

compd	R <sup>1</sup>	FGFR3 IC <sub>50</sub> (nM)	FGFR1 IC <sub>50</sub> (nM)
<b>6</b>	OMe	13	428
<b>7</b>	NHMe	34	420
<b>8</b>	OEt	56	477
<b>9</b>	O <i>i</i> -Pr	54	365
<b>10</b>	OPh	1177	2648
<b>11</b>	OBn	441	362
<b>12</b>	OCH <sub>2</sub> CH <sub>2</sub> N(Me) <sub>2</sub>	247	415

carried out interchangeably with the benzamide or *m*-pyridyl amide. The improvement in potency resulting from methoxy substitution at R<sup>1</sup> encouraged further exploration into this pocket. Initially, this region appeared intolerant of larger substituents, since a modest increase in size to the ethoxy derivative **8** led to a 3-fold loss in potency relative to **6** (FGFR3 IC<sub>50</sub> = 56 nM vs 13 nM). We probed for lipophilic or hydrophilic interactions by installing larger groups such as phenyl (**10**), benzyl (**11**), and diethylamino (**12**), but in all cases, significant losses in FGFR3 enzyme potency were observed.

The most critical trend in the SAR was the observation that expanding the ethoxy group to the more sterically encumbered isopropoxy group (**9**) did not negatively affect potency, suggesting that sp<sup>3</sup> rings might be tolerated in this region. To assess how we might capitalize on this observation, compound **9** was docked into the ATP binding site of FGFR3 (Figure 2) using a known crystal structure (PDB code: 4K33).<sup>15</sup> Our generated model showed two key interactions: the nitrogen of the imidazole ring forming a hydrogen bond to Ala558 in the hinge region and the amide carbonyl forming a hydrogen bond to Lys508 with the *N*-methyl group extending past the gatekeeper (Val555). Importantly, we noticed that the isopropyl group was situated close to an asparagine residue in the lower hinge region (Asn562, Figure 2a). The proximity of these substituents, in combination with the SAR, guided a design strategy aimed at delivering a heteroatom to engage the primary amide N–H of Asn562 in a hydrogen bonding interaction. To this end, the isopropyl group was cyclized to (hetero)cycloalkyl rings of varying size and substitution (Table 3).

The azetidine derivative **13** lost significant potency for FGFR3 (IC<sub>50</sub> = 515 nM), while the lactam **14** was better tolerated (FGFR3 IC<sub>50</sub> = 18 nM) but offered no improvement relative to **5**. Substitution with tetrahydropyran (**15**) also led to a significant loss of potency and selectivity. We were delighted to find that the oxetane derivative **16** improved the FGFR3

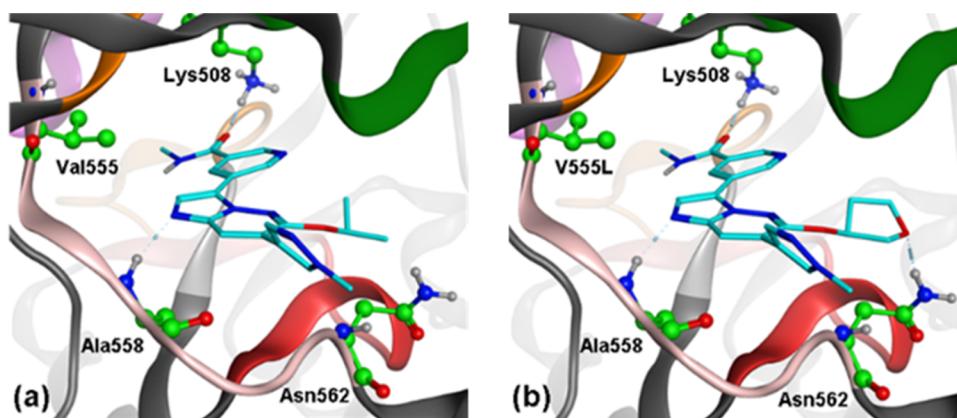


**Figure 2.** (a) MOE docking of **9** in apo FGFR3 (PDB ID: 4K33). (b) Design of the THF ether to engage Asn562 (PDB ID: 4K33).

**Table 3.** SAR of (Hetero)Cycloalkyl Ethers

Cmpd	R <sup>2</sup>	FGFR3 IC <sub>50</sub> (nM)	FGFR1 IC <sub>50</sub> (nM)	BA/F3 IC <sub>50</sub> (nM)
<b>13</b>		515	1683	
<b>14</b>		18	155	
<b>15</b>		167	283	
<b>16</b>		1.1	71	29
<b>17</b>		2.4	117	42
<b>18</b>		41	433	
<b>19</b>		0.9	30	15

potency (IC<sub>50</sub> = 1.1 nM) and further increased the selectivity over FGFR1 (65×). The racemic tetrahydrofuran (THF)-substituted compound **17** also enhanced the potency (FGFR3 IC<sub>50</sub> = 2.4 nM) and FGFR1 selectivity (R1/R3 = 49×). We prepared the single enantiomers of **17** and found that the (*S*)-enantiomer **19** was the active isomer. Compound **19** was the first in this series to display sub-nanomolar enzymatic potency (FGFR3 IC<sub>50</sub> = 0.9 nM). Given that FGFR1 also contains an asparagine residue at this position (Asn571), molecular modeling was ineffective at explaining the increase in selectivity for **19** relative to **5**. A slight conformational difference in the protein backbone could possibly make this interaction more favorable in FGFR3.

The most potent compounds (**16**, **17**, and **19**) were tested in a homogeneous time-resolved fluorescence (HTRF) cellular assay using TEL-FGFR3-BA/F3 cells, a functional assay measuring compound inhibition of phospho-FGFR3. In addition to the best FGFR3 potency, **19** also exhibited the most potent cellular activity (BA/F3 IC<sub>50</sub> = 15 nM).

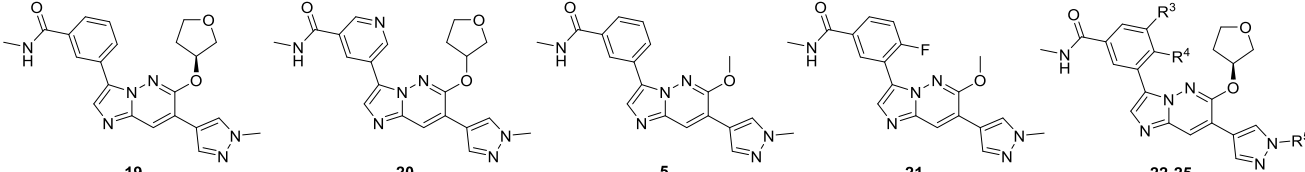
A broad in-house kinase panel screen of an early compound related to **4** identified four other kinases that were inhibited with IC<sub>50</sub> < 100 nM: PDGFRB, KIT, FLT3, and TRKA (data not shown). Unfortunately, **19** was found to have less than desirable selectivity over these kinases as well (Table 4). To mitigate the possibility of off-target toxicity, we desired 100-fold selectivity over all other kinases.

Replacement of the benzamide ring in **19** with *m*-pyridyl (compound **20**) dramatically improved kinase selectivity without affecting FGFR3 potency (FGFR3 IC<sub>50</sub> = 2.2 nM). However, compound **20** did not translate well from enzyme to cell (BA/F3 IC<sub>50</sub> = 969 nM), undoubtedly a result of poor cellular permeation due to high polarity (C log *P* = 0.02). Consequently, we were forced to identify an alternative solution for improving the kinase selectivity of **19**.

During the course of our work on exploring the ethers, a concurrent effort was undertaken to investigate substitution on the aromatic positions of the benzamide ring. Careful analysis of the SAR revealed two key trends: addition of fluorine *para* to the *N*-methyl amide (R<sup>4</sup>, Table 4) abolished potency toward KIT and PDGFRB (e.g., **5** → **21**), while substitution of a methyl group in the *meta* position (R<sup>3</sup>, Table 4) significantly reduced activity for FLT3 and TRKA (e.g., **19** → **22**). These trends suggested that incorporating benzamides with substitution at both R<sup>3</sup> and R<sup>4</sup> would result in compounds with desirable selectivity over all four problematic kinases.

Gratifyingly, the 4-fluoro-3-methylbenzamide compound **23** verified our hypothesis and demonstrated >100-fold kinome selectivity. Compound **23** also maintained excellent potency for FGFR3 (IC<sub>50</sub> = 0.7 nM) and selectivity over FGFR1 (62×). Compound **24**, a 3-difluoromethyl-4-fluorobenzamide, displayed a similar profile to **23** and maintained potent activity against the V555L (IC<sub>50</sub> = 2.6 nM) and V555M (IC<sub>50</sub> = 0.9 nM) GK mutants. The 3,4-difluorobenzamide derivative **25** had the best biochemical potency (FGFR3 IC<sub>50</sub> = 0.6 nM) and general kinase profile of the series. Notably, **25** (C log *P* = 1.2) is significantly less polar than **20**. This compound was very potent in the BA/F3 cellular assay (IC<sub>50</sub> = 6.8 nM) and was found to have highly desirable *in vitro* ADME properties (Table 5), with low intrinsic clearance (0.5 L/h/kg), high

Table 4. Phenyl Ring SAR and General Kinase Selectivity Data



cmpd	R <sup>3</sup>	R <sup>4</sup>	R <sup>5</sup>	FGFR3 IC <sub>50</sub> (nM)	FGFR1 IC <sub>50</sub> (nM)	FGFR3 V555L IC <sub>50</sub> (nM)	FGFR3 V555M IC <sub>50</sub> (nM)	BA/F3 IC <sub>50</sub> (nM)	FLT3 IC <sub>50</sub> (nM)	TRKA IC <sub>50</sub> (nM)	KIT IC <sub>50</sub> (nM)	PDGFRB IC <sub>50</sub> (nM)
19	H	H	Me	0.9	36	0.5		15	25	118	82	66
20		H	Me	2.2	147			969	1343	7304	384	370
5	H	H	Me	4.6	86			33	12	58	33	38
21	H	F	Me	2.6	60			14	8	11	180	348
22	Me	H	<i>i</i> -Pr	1.3	39	5.3	3.2	5.4	114	363	22	126
23	Me	F	Me	0.7	46			12	97	293	1657	1386
24	CHF <sub>2</sub>	F	Me	0.9	49	2.6	0.9	13	98	443	619	800
25	F	F	Me	0.6	21			6.8	155	285	1449	1741

Table 5. *In Vitro* ADME and Pharmacokinetics of 25 in Rat

**25**

Caco-2 ( $P_{app} \times 10^{-6}$ cm/s)	5.7
h-Cl (L/h/kg)	0.5
solubility ( $\mu$ g/mL, FASSIF/SGF)	118/>400
CYP3A4 IC <sub>50</sub> ( $\mu$ M)	3.9

rat i.v.

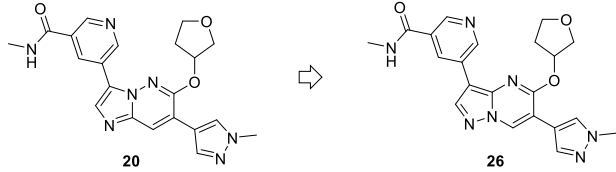
rat p.o.

dose (mg/kg)	0.73	dose (mg/kg)	3.1
HBf%	3.3	$C_{max}$ (nM)	6173
$V_{dss}$ (L/kg)	0.35	AUC (nM·h)	33 587
$T_{1/2}$ (h)	5.3	F%	54

Caco-2 permeability ( $P_{app} = 5.7 \times 10^{-6}$  cm/s), and good solubility (FASSIF/SGF = 118/>400  $\mu$ g/mL). On the basis of this profile, **25** was dosed in a rat PK cassette.

Upon i.v. dosing in rat, **25** exhibited very low clearance (HBF = 3.3%) and a moderate half-life ( $t_{1/2} = 5.3$  h). Oral dosing (p.o.) resulted in excellent exposure (AUC = 33 587 nM·h) with good oral bioavailability ( $F\% = 54$ ). Before examining pharmacokinetics in higher species, compound **25** was screened in a full cytochrome P450 (CYP) panel. Unfortunately, we found that **25** potently inhibited the activity of CYP3A4 (IC<sub>50</sub> = 3.9  $\mu$ M). It is also possible that the CYP inhibition contributed to the high exposure of **25**.

We revisited **20**, speculating that the additional polarity imparted by the *m*-pyridyl ring would reduce CYP inhibition. In fact, **20** had no effect on CYP3A4 (0% inhibition at 5  $\mu$ M, Table 6). Encouraged by this data, several approaches to improve the cell permeability of **20** were considered. One such strategy was to modulate the polarity of the bicyclic core. This was implemented by switching the position of the bridgehead nitrogen, thereby converting the highly basic imidazo[1,2-*b*]pyridazine core to a significantly less polar pyrazolo[1,5-*a*]pyrimidine. Pleasingly, the resulting compound **26** was 2-fold more potent than **20** in the enzyme assay (FGFR3 IC<sub>50</sub> = 1.0 nM vs 2.2 nM, respectively), with dramatically improved

Table 6. Comparison of Imidazo[1,2-*b*]Pyridazine and Pyrazolo[1,5-*a*]Pyrimidine Scaffolds


cmpd	FGFR3 IC <sub>50</sub> (nM) (R1/R3)	BA/F3 IC <sub>50</sub> (nM)	CYP3A4 IC <sub>50</sub> ( $\mu$ M) (%inh @ 5 $\mu$ M)	Caco-2 ( $P_{app} \times 10^{-6}$ cm/s)
20	2.2 (67 $\times$ )	969	>5 (0)	
26	1.0 (50 $\times$ )	29	>5 (15)	0.2

cellular translation (BA/F3 IC<sub>50</sub> = 29 nM vs 969 nM) and minimal CYP inhibition.

The low permeability of **26** ( $P_{app} = 0.2 \times 10^{-6}$  cm/s) was addressed by the replacement of the pyrazole *N*-methyl group with isopropyl to afford **27** ( $P_{app} = 1.5 \times 10^{-6}$  cm/s, Table 7). Compound **27** was among the most potent in the enzyme assay (FGFR3 IC<sub>50</sub> = 0.4 nM), with excellent potency in cells (BA/F3 IC<sub>50</sub> = 7.2 nM).

Despite the well-distributed and overall polarity of **27**, this compound still inhibited the activity of CYP3A4 (IC<sub>50</sub> = 9  $\mu$ M). At this point, we speculated that the CYP inhibition in this series might be due to specific heme binding rather than general lipophilicity.<sup>16</sup> A possible culprit was proposed to be the carbonyl of the *N*-methyl amide or the corresponding (presumed) primary amide metabolite. Increasing steric hindrance of the amide and/or blocking *N*-demethylation would be expected to disrupt this binding and mitigate CYP inhibition. To test these hypotheses, an *N*-ethyl derivative (**28**) and the *N*-CD<sub>3</sub> congener (**29**) of **27** were prepared (Table 7).<sup>17</sup> Pleasingly, both compounds had a clean CYP profile (CYP3A4 IC<sub>50</sub> >25  $\mu$ M). Compound **29** maintained the excellent potency and selectivity of **27**, while **28** was considerably less potent and selective (FGFR3 IC<sub>50</sub> = 2.6 nM, R1/R3 = 21 $\times$ ). The *in vitro* intrinsic clearance of **29** was also dramatically reduced compared to **27** (0.5 L/h/kg vs 1.0 L/h/kg, respectively), indicating *N*-demethylation as a likely site of metabolism. We developed a whole blood (WB) assay using FGFR3 RT-112/84 cells, in which **29** displayed excellent potency (WB IC<sub>50</sub> = 177 nM). On the basis of this profile, **29**



Table 7. Potency and *In Vitro* ADME Profile of Lead Compound 29

cmpd	FGFR3		FGFR3		FGFR3		BA/F3		WB		Caco-2 ( $P_{app} \times 10^{-6}$ cm/s)	h-Cl (L/h/kg)	CYP3A4 IC <sub>50</sub> ( $\mu$ M)	solubility ( $\mu$ g/mL) (FaSSIF/SGF)
	IC <sub>50</sub> (nM)	FGFR1 IC <sub>50</sub> (nM) (R1/R3)	FGFR3 V555L IC <sub>50</sub> (nM)	FGFR3 V555M IC <sub>50</sub> (nM)	IC <sub>50</sub> (nM)	IC <sub>50</sub> (nM)	IC <sub>50</sub> (nM)	IC <sub>50</sub> (nM)	IC <sub>50</sub> (nM)	IC <sub>50</sub> (nM)				
27	0.4	17 (43×)	1.8	5.2	7.2						1.5	1.0	9	17/>400
28	2.6	54 (21×)			22						0.6	1.0	>25	
29	0.5	21 (42×)	2.7	6.1	5.5	177					2.0	0.5	>25	18/679

was advanced into rat PK studies (Table 8). Clearance in the i.v. arm was low (HBF = 35%), with a moderate half-life ( $t_{1/2}$  =

Table 8. Pharmacokinetics of 29 in Rat

rat i.v.		rat p.o.	
dose (mg/kg)	1.0	dose (mg/kg)	3.0
HBF%	35	C <sub>max</sub> (nM)	2303
V <sub>ds</sub> (L/kg)	1.6	AUC (nM·h)	5108
T <sub>1/2</sub> (h)	1.7	F%	82

1.7 h). In the p.o. dose, 29 demonstrated good exposure (AUC = 5108 nM·h) and high oral bioavailability (F% = 82). Compound 29 was tested for activity toward several FGFR3 gatekeeper mutants. Despite the fact that nearly all compounds tested in this series were equipotent for the GK mutants, 29 lost 5-fold potency for the V555L mutant (IC<sub>50</sub> = 2.7 nM) and 10-fold potency for the V555M mutant (IC<sub>50</sub> = 6.1 nM).

Screening an additional diverse set of compounds from these series revealed that pyridine nitrogen was responsible for this loss in activity. To understand this result, we obtained an X-ray co-crystal structure of an analogous compound (30) bound to FGFR2 (Figure 3). This isoform was more amenable to

crystallization than FGFR3, and 30 was confirmed to have identical biochemical potency in both. Contrary to our initial docking model, the pyridyl ring is flipped, with the amide extending toward the ATP sugar pocket and the pyridine nitrogen oriented toward the gatekeeper residue. It appears that the larger, more lipophilic groups of the FGFR3 V555L and V555M mutants clash with the polar nitrogen of the pyridyl ring, thereby resulting in the observed loss in potency. Notably, the oxygen of the THF ring forms a hydrogen bonding interaction with the primary amide N–H of Asn571 as designed (for Asn562 in FGFR3).

We further profiled 29 against the other FGFR isoforms (FGFR2/4) in addition to the approved inhibitors 1–3 (Table 9). Compound 29 was found to be equally potent for FGFR2 (IC<sub>50</sub> = 1.0 nM) and highly selective over FGFR4 (IC<sub>50</sub> = 145 nM). As expected, 1–3 maintained equal potency for FGFR1 with >50-fold loss in activity for the FGFR3 V555L and V555M GK mutants. Collectively, this data demonstrates that our novel compounds are isoform-selective inhibitors of FGFR2/3 with significantly improved potency toward the common GK mutations, in contrast to first-generation pan-FGFR inhibitors.

Furthermore, 29 also maintained >100-fold selectivity against all 36 structurally representative kinases from an in-house kinase panel (Table S1).

Prior to the discovery of 29, compound 27 was dosed in an *in vivo* pharmacodynamic study to measure both the inhibition of FGFR pathway as well as the induction of phosphorous in mice. First, we determined the percent inhibition of pERK in the UM-UC-14 human bladder cell carcinoma model.<sup>18,19</sup> Tumor-bearing mice were dosed by oral gavage with 27 or pemigatinib, and tumors were analyzed 2 h post-dose administration. The data show a dose-dependent target inhibition of pERK by 27, with maximal inhibition observed at the high dose (100 mg/kg) and comparable to a high dose of 10 mg/kg pemigatinib (Figure 4). Importantly, 27 did not significantly increase phosphorus levels in serum at any of the doses tested when compared to vehicle control. In contrast, a high single dose of 10 mg/kg pemigatinib was sufficient to

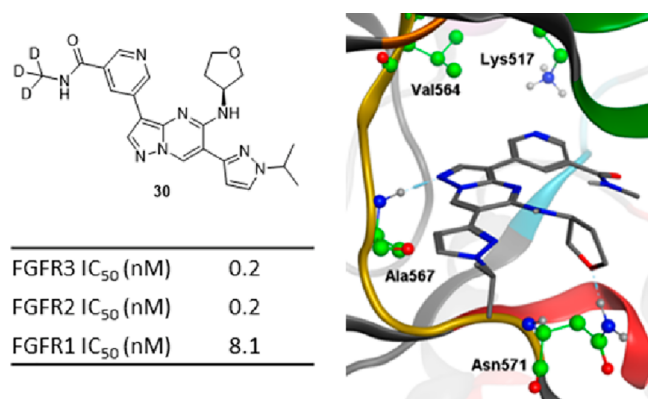
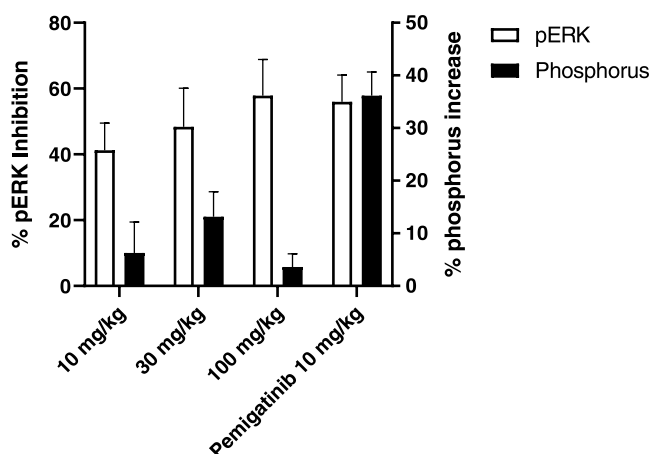


Figure 3. X-ray co-crystal structure of 30 in FGFR2 (PDB code: 8E1X).

Table 9. Comparison of Novel FGFR2/3 Inhibitor 29 and Approved FGFR Inhibitors 1–3

compound	FGFR1 IC <sub>50</sub> (nM)	FGFR2 IC <sub>50</sub> (nM)	FGFR3 IC <sub>50</sub> (nM)	FGFR4 IC <sub>50</sub> (nM)	FGFR3 V555L IC <sub>50</sub> (nM)	FGFR3 V555M IC <sub>50</sub> (nM)
29	21	1.0	0.5	145	2.7	6.1
erdafitinib (1)	0.2	0.2	0.6	1.9	21	68
pemigatinib (2)	0.9	0.4	1.7	27	373	201
infigratinib (3)	2.1		2.7	115	3036	352



**Figure 4.** Percentages of pERK inhibition and phosphorus increase induced by **27** compared to vehicle control.

significantly increase phosphorus levels by 36%, further supporting the importance of a selective FGFR3 inhibitor.

## CONCLUSIONS

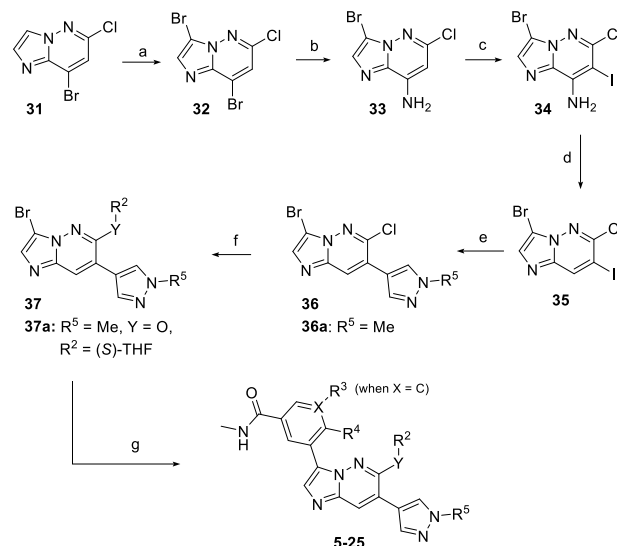
In summary, the hit to lead development of next-generation FGFR2/3 inhibitors has been disclosed. Key discoveries include the THF-substituted ether to drive potency into sub-nanomolar range, the 4-fluoro-3-substituted benzamides to improve general kinase selectivity, a scaffold hop to reduce the polarity of the bicyclic core and enhance cellular permeability, and replacement of the *N*-methyl amide with *N*-CD<sub>3</sub> to shut down a (presumed) metabolic pathway and abolish CYP3A4 inhibition. The lead compound **29** is a highly potent inhibitor of FGFR2/3, has excellent FGFR1/4 and kinome selectivity, as well as desirable *in vitro* ADME properties and pharmacokinetics in rat. An X-ray co-crystal structure of a related compound showed orientation of the pyridine nitrogen toward the gatekeeper residue, explaining the slight loss in potency for the V555L and V555M mutants. A combined PD/serum phosphate-level study established that toxicity caused by hyperphosphatemia could potentially be avoided in a clinical setting with FGFR2/3 inhibitors that have high selectivity over FGFR1.

## CHEMISTRY

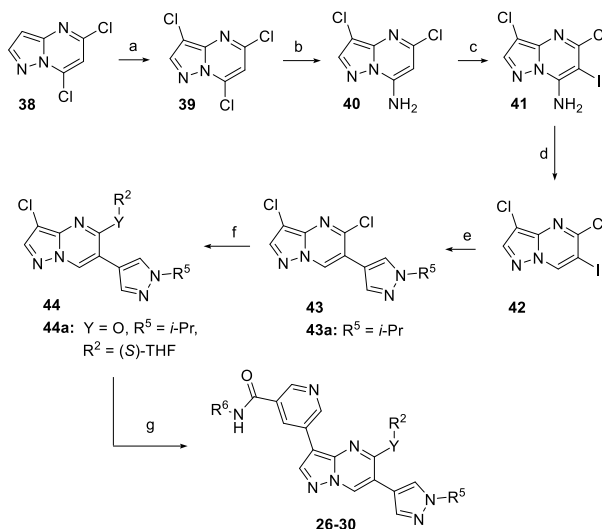
Compounds **5–25** were synthesized according to the synthetic route outlined in Scheme 1. Bromination of commercially available imidazo[1,2-*b*]pyridazine **31** with *N*-bromosuccinimide affords the trihalogenated intermediate **32** in nearly quantitative yield. Selective S<sub>N</sub>Ar with NH<sub>4</sub>OH then provides amine **33**, which is selectively halogenated with *N*-iodosuccinimide to deliver **34**. Removal of the amino group by heating with *t*-BuONO leads to key intermediate **35** via diazotization and loss of N<sub>2</sub>. A selective Suzuki coupling of the iodide over the bromide affords pyrazole **36**. Reaction of **36** with the appropriate alcohols and Cs<sub>2</sub>CO<sub>3</sub> in DMF at 90 °C provides intermediates **37**, which undergo a second Suzuki coupling to install the (un)substituted benzamide rings or the *m*-pyridyl derivatives. Notably, displacement of the chloride in **36** with amines required heating at 160 °C in NMP.

Compounds **26–30** were synthesized according to the synthetic route outlined in Scheme 2. Chlorination of commercially available pyrazolo[1,5-*a*]pyrimidine **38** with *N*-chlorosuccinimide affords trichlorinated intermediate **39**,

Scheme 1. (a) NBS, DMF, 60 °C, 2 h, quant.; (b) aq. NH<sub>4</sub>OH, sealed vessel, 120 °C, 81%; (c) NIS, DMF, 60 °C, 2 h, quant.; (d) *t*-BuONO, THF, 70 °C, 2 h, 81%; (e) ArB(OH)<sub>2</sub> or ArBPin, K<sub>2</sub>CO<sub>3</sub>, Pd(PPh<sub>3</sub>)<sub>4</sub>, 5:1 1,4-dioxane/water, 100 °C, 16 h, 81%; (f) R<sup>2</sup>OH, Cs<sub>2</sub>CO<sub>3</sub>, DMF, 90 °C, 1 h when Y = O; R<sup>2</sup>NH<sub>2</sub>, Cs<sub>2</sub>CO<sub>3</sub>, NMP, 160 °C, 1 h when Y = N; and (g) ArB(OH)<sub>2</sub> or ArBPin, Na<sub>2</sub>CO<sub>3</sub>, Pd(dppf)Cl<sub>2</sub>·CH<sub>2</sub>Cl<sub>2</sub>, 3:1 DMF/water or 3:1 dioxane/water, 90 °C, 2 h



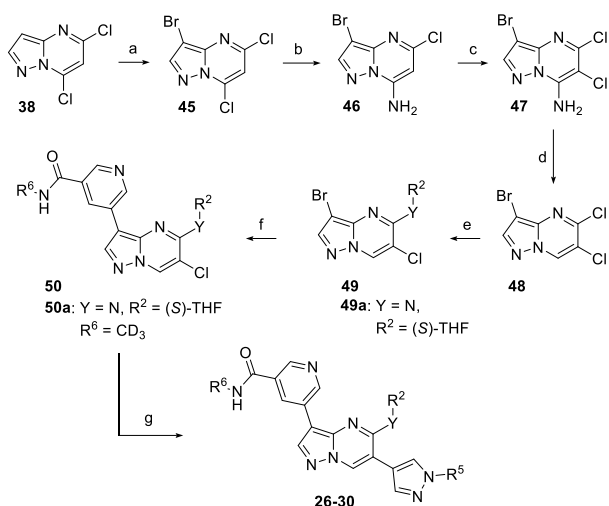
Scheme 2. (a) NCS, DMF, 60 °C, 2 h, 78%; (b) aq. NH<sub>4</sub>OH, sealed vessel, 100 °C, 85%; (c) NIS, DMF, 60 °C, 2 h, 85%; (d) *t*-BuONO, THF, 70 °C, 2 h, 47%; (e) ArB(OH)<sub>2</sub> or ArBPin, K<sub>2</sub>CO<sub>3</sub>, PdCl<sub>2</sub>(dppf)·CH<sub>2</sub>Cl<sub>2</sub>, 5:1 1,4-dioxane/water, 100 °C, 1 h; (f) R<sup>2</sup>OH or R<sup>2</sup>NH<sub>2</sub>, Cs<sub>2</sub>CO<sub>3</sub>, DMF, 90 °C, 1 h; and (g) ArB(OH)<sub>2</sub> or ArBPin, Cs<sub>2</sub>CO<sub>3</sub>, XPhos Pd G2, 3:1 DMF/water or 3:1 dioxane/water, 90 °C, 2 h



which undergoes selective S<sub>N</sub>Ar to give amine **40**. Iodination with *N*-iodosuccinimide cleanly provides **41**, which is deaminated by heating with *t*-BuONO in THF. Selective Suzuki coupling of the iodide then delivers pyrazole **43**. Reaction of **43** with ethers or amines and cesium carbonate at elevated temperature provides intermediates **44**, which undergo a second Suzuki coupling to install the amide-substituted aryl ring.

Alternatively, compounds **26–30** may be prepared by a modified route outlined in Scheme 3. In this case, the initial halogen introduced is a bromo, which ultimately allows the pyridyl ring to be installed first.

**Scheme 3.** (a) NBS, DMF, 2 h, 86%; (b) aq.  $\text{NH}_4\text{OH}$ , sealed vessel, 100 °C, 98%; (c) NCS, DMF, 50 °C, 0.5 h, 82%; (d)  $t\text{-BuONO}$ , THF, 70 °C, 2 h, 64%; (e)  $\text{R}^2\text{OH}$  or  $\text{R}^2\text{NH}_2$ ,  $\text{Cs}_2\text{CO}_3$ , DMF, 90 °C, 1 h; (f)  $\text{ArB}(\text{OH})_2$  or  $\text{ArBPin}$ ,  $\text{K}_2\text{CO}_3$ ,  $\text{PdCl}_2(\text{dppf})\cdot\text{CH}_2\text{Cl}_2$ , 4:1 1,4-dioxane/water, 100 °C, 1 h; and (g)  $\text{ArB}(\text{OH})_2$  or  $\text{ArBPin}$ ,  $\text{Cs}_2\text{CO}_3$ , XPhos Pd G2, 3:1 DMF/water or 3:1 dioxane/water, 90 °C, 2 h



## EXPERIMENTAL SECTION

All reactions were run under an atmosphere of dry nitrogen. Unless otherwise noted, all reactions were performed at ambient temperature, which averaged 20 °C. All solvents were used without further purification as acquired from commercial sources. NMR spectra were obtained using a Varian Mercury-300, Mercury-400, or Inova-500 spectrometer. Chemical shifts are reported in parts per million relative to tetramethylsilane (TMS) as internal standard. All final products were characterized by  $^1\text{H}$  NMR, HRMS or LCMS, and HPLC methods. Purifications by flash chromatography were performed on RediSep columns using an Isco CombiFlash SG100c. Reverse-phase preparative HPLC purifications were performed on Waters FractionLynx system using UV-triggered or mass-directed fractionation and compound-specific method optimization.<sup>20</sup> All final compounds for biological testing were purified by reverse-phase prep HPLC to >95% purity, as determined by analytical LCMS.

**Synthesis of Compound 25.** **Step 1.** 3,8-Dibromo-6-chloroimidazo[1,2-*b*]pyridazine (**32**). 8-Bromo-6-chloroimidazo[1,2-*b*]pyridazine (10.6 g, 45.8 mmol) was dissolved in DMF (114 mL) and treated with NBS (10.6 g, 59.5 mmol). The solution was stirred at 60 °C. After 2 h, LCMS indicated complete consumption of the starting material. The reaction was poured into ice water (800 mL) and stirred for 1 h at room temperature. The mixture was filtered under vacuum, and the residue was dried with continued air flow to provide 3,8-dibromo-6-chloroimidazo[1,2-*b*]pyridazine (14.8 g, 47.5 mmol, quantitative yield assumed). The crude material was used without further purification. LCMS calculated for  $\text{C}_6\text{H}_3\text{Br}_2\text{ClN}_3$  ( $M + \text{H}$ )<sup>+</sup>:  $m/z = 311.8, 309.8, 313.8$ ; found: 311.8, 309.8, 313.8.

**Step 2.** 3-Bromo-6-chloroimidazo[1,2-*b*]pyridazin-8-amine (**33**). 3,8-Dibromo-6-chloroimidazo[1,2-*b*]pyridazine (14.8 g, 47.5 mmol) was placed in a 350 mL heavy-walled pressure vessel with a stir bar. This sample was treated with aqueous ammonium hydroxide (111 mL, 2.85 mol), the chamber was sealed, and the heterogeneous mixture was warmed to 120 °C. After 4 h, the reaction was cooled to

room temperature, carefully opened, and an LCMS aliquot indicated complete consumption of the starting material. The mixture was poured into 800 mL of ice water and stirred for an hour at room temperature. The mixture was filtered under vacuum, and the residue was dried with continued air flow to provide 3-bromo-6-chloroimidazo[1,2-*b*]pyridazin-8-amine (9.5 g, 38 mmol, 81%). The crude material was used without further purification. LCMS calculated for  $\text{C}_6\text{H}_3\text{BrClN}_4$  ( $M + \text{H}$ )<sup>+</sup>:  $m/z = 246.9, 248.9$ ; found: 246.9, 248.9.

**Step 3.** 3-Bromo-6-chloro-7-iodoimidazo[1,2-*b*]pyridazin-8-amine (**34**). 3-Bromo-6-chloroimidazo[1,2-*b*]pyridazin-8-amine (6.8 g, 28 mmol) was dissolved in DMF (69 mL) and treated with *N*-iodosuccinimide (10.5 g, 46.7 mmol). The solution was stirred at 60 °C. After 2 h, LCMS indicated complete consumption of the starting material. The reaction was poured into ice water (500 mL) and stirred for an hour at room temperature. The mixture was filtered under vacuum, and the residue was dried with continued air flow to provide the title compound (11.6 g, 31.1 mmol, quantitative yield assumed). The crude material was used without further purification. LCMS calculated for  $\text{C}_6\text{H}_4\text{BrClIN}_4$  ( $M + \text{H}$ )<sup>+</sup>:  $m/z = 372.8, 374.8$ ; found: 372.8, 374.8.

**Step 4.** 3-Bromo-6-chloro-7-iodoimidazo[1,2-*b*]pyridazine (**35**). 3-Bromo-6-chloro-7-iodoimidazo[1,2-*b*]pyridazin-8-amine (10.3 g, 27.5 mmol) was placed in a 350 mL heavy-walled pressure vessel and dissolved in THF (83 mL). The sample was treated with salicylic acid (0.76 g, 5.5 mmol) and *tert*-butyl nitrite (36.3 mL, 275 mmol), and the vessel was sealed. The reaction was warmed to 70 °C. After 2 h, LCMS indicated complete consumption of the starting material. The solution was cooled to room temperature and concentrated *in vacuo*. The residue was dissolved in EtOAc, adsorbed onto silica, and purified by flash chromatography in 0–50% EtOAc/hexanes to provide the title compound (7.95 g, 22.2 mmol, 81%). LCMS calculated for  $\text{C}_6\text{H}_3\text{BrClIN}_3$  ( $M + \text{H}$ )<sup>+</sup>:  $m/z = 357.8, 359.8$ ; found: 357.8, 359.8.

**Step 5.** 3-Bromo-6-chloro-7-(1-methyl-1*H*-pyrazol-4-yl)imidazo[1,2-*b*]pyridazine (**36a**). A sample of 3-bromo-6-chloro-7-iodoimidazo[1,2-*b*]pyridazine (1.4 g, 3.9 mmol) was dissolved in 1,4-dioxane (16 mL) and was treated with  $\text{K}_2\text{CO}_3$  (1.08 g, 7.81 mmol), water (3.3 mL), and 1-methyl-4-(4,4,5,5-tetramethyl-1,3,2-dioxaborolan-2-yl)-1*H*-pyrazole (853 mg, 4.10 mmol). This solution was degassed with bubbling nitrogen for 5 min. Tetrakis-(triphenylphosphine)palladium(0) (0.45 g, 0.39 mmol) was added, the vial was capped, and the solution was stirred at 100 °C. After 16 h, LCMS indicated ~85% conversion. The solution was cooled to room temperature, quenched with aqueous  $\text{NH}_4\text{Cl}$ , and extracted with EtOAc, then with 25% *iso*-propanol in chloroform. The combined organic fractions were dried over  $\text{MgSO}_4$ , filtered, and concentrated *in vacuo*. The crude sample was purified by flash chromatography in 0–100% EtOAc/DCM and then in 0–10% MeOH/DCM to provide the title compound (7.95 g, 22.2 mmol, 81%). LCMS calculated for  $\text{C}_{10}\text{H}_8\text{BrClN}_5$  ( $M + \text{H}$ )<sup>+</sup>:  $m/z = 312.0, 314.0$ ; found: 311.8, 313.8.

**Step 6.** (S)-3-Bromo-7-(1-methyl-1*H*-pyrazol-4-yl)-6-((tetrahydrofuran-3-yl)oxy)imidazo[1,2-*b*]pyridazine (**37a**). A sample of 3-bromo-6-chloro-7-(1-methyl-1*H*-pyrazol-4-yl)imidazo[1,2-*b*]pyridazine (218 mg, 0.70 mmol) was dissolved in 1,4-dioxane (8.7 mL) and was treated with cesium carbonate (682 mg, 2.09 mmol) and (S)-tetrahydrofuran-3-ol (846  $\mu\text{L}$ , 10.5 mmol). This solution was stirred at 110 °C. After 16 h, LCMS indicated complete consumption of the starting material. The solution was cooled to room temperature, quenched with aqueous  $\text{NH}_4\text{Cl}$ , and the mixture was extracted with EtOAc. The combined organic fractions were dried over  $\text{MgSO}_4$ , filtered, and concentrated *in vacuo*. The crude material was flashed in 0–100% EtOAc/DCM and then in 0–10% MeOH/DCM to afford the title compound (188 mg, 74%). LCMS calculated for  $\text{C}_{14}\text{H}_{15}\text{BrN}_5\text{O}_2$  ( $M + \text{H}$ )<sup>+</sup>:  $m/z = 364.0, 366.0$ ; found: 364.2, 366.2.

**Step 7.** (S)-3,4-Difluoro-*N*-methyl-5-(7-(1-methyl-1*H*-pyrazol-4-yl)-6-((tetrahydrofuran-3-yl)oxy)imidazo[1,2-*b*]pyridazin-3-yl)-benzamide (**25**). (S)-3-Bromo-7-(1-methyl-1*H*-pyrazol-4-yl)-6-((tetrahydrofuran-3-yl)oxy)imidazo[1,2-*b*]pyridazine (34 mg, 0.09 mmol) was dissolved in DMF (1.5 mL) and was treated with  $\text{K}_2\text{CO}_3$  (38 mg, 0.3 mmol), water (0.3 mL), and 3,4-difluoro-*N*-methyl-5-(4,4,5,5-



tetramethyl-1,3,2-dioxaborolan-2-yl)benzamide (83 mg, 28  $\mu$ mol). This solution was degassed with bubbling nitrogen for 5 min. XPhos Pd G2 (11 mg, 14  $\mu$ mol) was added, the vial was capped, and the solution was stirred at 85 °C. After 2 h, LCMS indicated complete consumption of the starting material. The solution was cooled to room temperature, diluted with MeCN and water, filtered through a thiol SiliaPrep cartridge, and purified by HPLC (pH = 2) to provide the title compound (1.3 mg, 3%). LCMS calculated for  $C_{22}H_{21}F_2N_6O_3$  ( $M + H$ )<sup>+</sup>:  $m/z$  = 455.2; found: 455.4. <sup>1</sup>H NMR (600 MHz, DMSO-*d*<sub>6</sub>)  $\delta$  8.76 (d,  $J$  = 5.9 Hz, 1H), 8.60 (q,  $J$  = 4.7 Hz, 1H), 8.46 (s, 1H), 8.28 (s, 1H), 8.17 (s, 1H), 8.12 (s, 1H), 7.91 (m, 1H), 5.61 (m, 1H), 4.08 (d,  $J$  = 10.7 Hz, 1H), 4.04 (dd,  $J$  = 10.8, 4.6 Hz, 1H), 3.95 (m, 1H), 3.93 (s, 3H), 3.82 (dt,  $J$  = 4.9, 8.2 Hz, 1H), 2.81 (d,  $J$  = 4.5 Hz, 3H), 2.38 (m, 1H), 2.32 (m, 1H).

**Synthesis of Compound 27.** *Step 1.* 3,5,7-Trichloropyrazolo[1,5-*a*]pyrimidine (39). To a solution of 5,7-dichloropyrazolo[1,5-*a*]pyrimidine (500 mg, 2.66 mmol, Combi-Blocks ST-4256) in DMF (5 mL) was added NCS (391 mg, 2.93 mmol), and the reaction mixture was stirred at 60 °C for 1 h. After cooling to room temperature, ice chips and water were added. The resulting precipitate was filtered, washed with water, and air-dried to afford the title compound (460 mg, 78%) as an off-white solid. LCMS calculated for  $C_6H_3Cl_3N_3$  ( $M + H$ )<sup>+</sup>:  $m/z$  = 221.9; found: 221.9.

*Step 2.* Dichloropyrazolo[1,5-*a*]pyrimidin-7-amine (40). A suspension of 3,5,7-trichloropyrazolo[1,5-*a*]pyrimidine (460 mg, 2.07 mmol) in concentrated ammonium hydroxide (10 mL, 145 mmol) was heated to 100 °C in a heavy-walled sealed tube for 1 h. After cooling to room temperature, the reaction mixture was diluted with cold water and filtered. The collected solid was then washed with cold water and air-dried to afford the title compound (355 mg, 85%). LCMS calculated for  $C_6H_5Cl_2N_4$  ( $M + H$ )<sup>+</sup>:  $m/z$  = 203.0; found: 203.0.

*Step 3.* 3,5-Dichloro-6-iodopyrazolo[1,5-*a*]pyrimidin-7-amine (41). To a solution of 3,5-dichloropyrazolo[1,5-*a*]pyrimidin-7-amine (355 mg, 1.75 mmol) in DMF (5 mL) was added NIS (590 mg, 2.62 mmol), and the reaction mixture was stirred at 50 °C for 1 h. After cooling to room temperature, ice chips and water were added. The resulting precipitate was filtered, washed with water, and air-dried to afford the title compound (489 mg, 85%). LCMS calculated for  $C_6H_4Cl_2IN_4$  ( $M + H$ )<sup>+</sup>:  $m/z$  = 328.9; found: 328.8.

*Step 4.* 3,5-Dichloro-6-iodopyrazolo[1,5-*a*]pyrimidine (42). To a solution of 3,5-dichloro-6-iodopyrazolo[1,5-*a*]pyrimidin-7-amine (489 mg, 1.49 mmol) in THF (4 mL) was added *tert*-butyl nitrite (0.88 mL, 7.43 mmol), and the reaction mixture was heated to 80 °C for 2 h. The reaction mixture was concentrated and purified by flash chromatography (0–50% EtOAc/hexanes) to afford the title compound (217 mg, 47%). LCMS calculated for  $C_6H_3Cl_2IN_3$  ( $M + H$ )<sup>+</sup>:  $m/z$  = 313.9; found: 313.7.

*Step 5.* Dichloro-6-(1-isopropyl-1H-pyrazol-4-yl)pyrazolo[1,5-*a*]pyrimidine (43a). A mixture of 3,5-dichloro-6-iodopyrazolo[1,5-*a*]pyrimidine (100 mg, 0.32 mmol), 1-isopropyl-4-(4,4,5,5-tetramethyl-1,3,2-dioxaborolan-2-yl)-1H-pyrazole (75 mg, 0.32 mmol), Pd(dppf)Cl<sub>2</sub>·CH<sub>2</sub>Cl<sub>2</sub> (13 mg, 16  $\mu$ mol), and sodium carbonate (101 mg, 0.96 mmol) in 1,4-dioxane (2 mL) and water (0.5 mL) was sparged with N<sub>2</sub> and heated to 80 °C for 1 h. The reaction mixture was diluted with EtOAc and water. The layers were separated, and the organic layer was washed with brine, dried over MgSO<sub>4</sub>, filtered, and concentrated. The residue was purified by flash chromatography (0–100% EtOAc/hexanes) to afford the title compound (77 mg, 82%). LCMS calculated for  $C_{12}H_{12}Cl_2N_5$  ( $M + H$ )<sup>+</sup>:  $m/z$  = 296.0; found: 296.2.

*Step 6.* (S)-3-Chloro-6-(1-isopropyl-1H-pyrazol-4-yl)-5-((tetrahydrofuran-3-yl)oxy)pyrazolo[1,5-*a*]pyrimidine (44a). To a solution of 3,5-dichloro-6-(1-isopropyl-1H-pyrazol-4-yl)pyrazolo[1,5-*a*]pyrimidine (10 mg, 34  $\mu$ mol) in DMF (1 mL) was added (S)-tetrahydrofuran-3-ol (14 mg, 0.17 mmol), followed by cesium carbonate (16.5 mg, 0.051 mmol) at room temperature. The reaction mixture was heated to 80 °C for 1 h, then cooled to room temperature. The solution of the product in DMF was used directly

for the next reaction. LCMS calculated for  $C_{16}H_{19}ClN_5O_2$  ( $M + H$ )<sup>+</sup>:  $m/z$  = 348.1; found: 348.1.

*Step 7.* (S)-5-(6-(1-isopropyl-1H-pyrazol-4-yl)-5-((tetrahydrofuran-3-yl)oxy)pyrazolo[1,5-*a*]pyrimidin-3-yl)-N-methylnicotinamide (27). A mixture of (S)-3-chloro-6-(1-isopropyl-1H-pyrazol-4-yl)-5-((tetrahydrofuran-3-yl)oxy)pyrazolo[1,5-*a*]pyrimidine (12 mg, 35  $\mu$ mol), N-methyl-5-(4,4,5,5-tetramethyl-1,3,2-dioxaborolan-2-yl)-nicotinamide (11 mg, 41  $\mu$ mol), XPhos Pd G2 (1.4 mg, 1.7  $\mu$ mol), and cesium carbonate (34 mg, 0.1 mmol) in DMF (1 mL) and water (0.5 mL) was sparged with N<sub>2</sub> and heated to 100 °C for 2 h. The reaction was diluted with MeOH and filtered through a SiliaPrep thiol cartridge, and the product was purified by prep HPLC (pH 2) to provide the title compound (1.4 mg, 3.1  $\mu$ mol, 9% over two steps). LCMS calculated for  $C_{23}H_{26}N_7O_3$  ( $M + H$ )<sup>+</sup>:  $m/z$  = 448.2; found: 448.4. <sup>1</sup>H NMR (500 MHz, DMSO-*d*<sub>6</sub>)  $\delta$  9.39 (d,  $J$  = 2.1 Hz, 1H), 9.38 (s, 1H), 9.00 (t,  $J$  = 2.1 Hz, 1H), 8.85 (d,  $J$  = 2.0 Hz, 1H), 8.74 (s, 1H), 8.72 (q,  $J$  = 4.9, 4.4 Hz, 1H), 8.28 (s, 1H), 8.06 (s, 1H), 5.79 (td,  $J$  = 4.7, 2.4 Hz, 1H), 4.58 (p,  $J$  = 6.7 Hz, 1H), 4.17 (dd,  $J$  = 10.7, 4.7 Hz, 1H), 4.11–4.05 (m, 1H), 3.96 (q,  $J$  = 8.1 Hz, 1H), 3.88 (td,  $J$  = 8.3, 4.7 Hz, 1H), 2.86 (d,  $J$  = 4.5 Hz, 3H), 2.46 (dt,  $J$  = 14.6, 7.3 Hz, 1H), 2.36–2.26 (m, 1H), 1.47 (d,  $J$  = 6.6 Hz, 6H).

**Synthesis of Compound 29.** A mixture of (S)-3-chloro-6-(1-isopropyl-1H-pyrazol-4-yl)-5-((tetrahydrofuran-3-yl)oxy)pyrazolo[1,5-*a*]pyrimidine (44a, 150 mg, 0.43 mmol), N-(methyl-*d*<sub>3</sub>)-5-(4,4,5,5-tetramethyl-1,3,2-dioxaborolan-2-yl)nicotinamide (137 mg, 0.52 mmol, see the [Supporting Information](#) for preparation), XPhos Pd G2 (17 mg, 22  $\mu$ mol), and cesium carbonate (422 mg, 1.29 mmol) in 1,4-dioxane (4 mL) and water (0.5 mL) was sparged with N<sub>2</sub> and heated to 100 °C for 2 h. The reaction mixture was diluted with MeOH and filtered through a SiliaPrep thiol cartridge, and the residue was purified by prep HPLC (pH 2) to afford the title compound (73 mg, 38%). LCMS calculated for  $C_{23}H_{23}D_3N_7O_3$  ( $M + H$ )<sup>+</sup>:  $m/z$  = 451.2; found: 451.2. <sup>1</sup>H NMR (600 MHz, DMSO-*d*<sub>6</sub>)  $\delta$  9.40 (s, 2H), 8.99 (t,  $J$  = 2.2 Hz, 1H), 8.84 (s, 1H), 8.75 (s, 1H), 8.68 (s, 1H), 8.29 (s, 1H), 8.07 (s, 1H), 5.80 (ddt,  $J$  = 6.7, 4.4, 2.0 Hz, 1H), 4.59 (hept,  $J$  = 6.7 Hz, 1H), 4.18 (dd,  $J$  = 10.7, 4.8 Hz, 1H), 4.08 (dd,  $J$  = 10.7, 1.9 Hz, 1H), 3.96 (q,  $J$  = 7.9 Hz, 1H), 3.88 (td,  $J$  = 8.4, 4.7 Hz, 1H), 2.50–2.42 (m, 1H), 2.32 (dddd,  $J$  = 13.9, 6.9, 4.7, 1.9 Hz, 1H), 1.47 (d,  $J$  = 6.7 Hz, 6H).

**Synthesis of Compound 30.** *Step 1.* 3-Bromo-5,7-dichloropyrazolo[1,5-*a*]pyrimidine (45). To a solution of 5,7-dichloropyrazolo[1,5-*a*]pyrimidine (2.0 g, 10.6 mmol) in DMF (20 mL) was added NBS (2.1 g, 11.7 mmol), and the reaction mixture was stirred at room temperature for 1 h. Water was added, and the resulting precipitate was filtered, washed with water, and air-dried overnight to afford the title compound (2.43 g, 86%). The product was used without purification. LCMS calculated for  $C_6H_3BrCl_2N_3$  ( $M + H$ )<sup>+</sup>:  $m/z$  = 265.9; found: 265.9.

*Step 2.* 3-Bromo-5-chloropyrazolo[1,5-*a*]pyrimidin-7-amine (46). A suspension of 3-bromo-5,7-dichloropyrazolo[1,5-*a*]pyrimidine (2.4 g, 9.0 mmol) in concentrated ammonium hydroxide (30 mL, 0.4 mol) was heated to 100 °C in a heavy-walled sealed tube for 1 h. After cooling to room temperature, the reaction mixture was diluted with cold water and filtered. The collected solid was then washed with ice-cold water and air-dried to afford the title compound (2.19 g, 98%). LCMS calculated for  $C_6H_5BrClN_4$  ( $M + H$ )<sup>+</sup>:  $m/z$  = 246.9; found: 246.9.

*Step 3.* 3-Bromo-5,6-dichloropyrazolo[1,5-*a*]pyrimidin-7-amine (47). To a solution of 3-bromo-5-chloropyrazolo[1,5-*a*]pyrimidin-7-amine (2.19 g, 8.85 mmol) in DMF (20 mL) was added NCS (1.18 g, 8.85 mmol), and the reaction mixture was stirred at 50 °C for 1 h. After cooling to room temperature, ice chips and water were added, and the resulting precipitate was filtered, washed with water, and air-dried to afford the title compound (2.08 g, 82%). LCMS calculated for  $C_6H_4BrCl_2N_4$  ( $M + H$ )<sup>+</sup>:  $m/z$  = 280.9; found: 280.9.

*Step 4.* 3-Bromo-5,6-dichloropyrazolo[1,5-*a*]pyrimidine (48). To a solution of 3-bromo-5,6-dichloropyrazolo[1,5-*a*]pyrimidin-7-amine (11 g, 39 mmol) in THF (100 mL) was added *tert*-butyl nitrite (23 mL, 0.2 mol), and the reaction mixture was heated to 80 °C for 2 h. The reaction mixture was concentrated, loaded directly onto silica gel,



and purified by flash chromatography (0–20% EtOAc/hexanes) to afford the title compound (6.7 g, 64%).

**Step 5.** (S)-3-Bromo-6-chloro-N-(tetrahydrofuran-3-yl)pyrazolo[1,5-a]pyrimidin-5-amine (**49a**). A mixture of 3-bromo-5,6-dichloropyrazolo[1,5-a]pyrimidine (500 mg, 1.87 mmol), (S)-tetrahydrofuran-3-amine (485  $\mu$ L, 5.62 mmol), and cesium carbonate (732 mg, 2.25 mmol) in THF (6 mL) was heated to 80 °C for 2 h. The reaction mixture was cooled to room temperature, diluted with EtOAc, and filtered. The filtrate was concentrated *in vacuo*, and the residue was purified by flash chromatography (0–50% EtOAc/hexanes) to afford the title compound (414 mg, 70%) as a light yellow solid. LCMS calculated for  $C_{10}H_{11}BrClN_4O$  ( $M + H$ )<sup>+</sup>:  $m/z$  = 317.0; found: 316.8.

**Step 6.** (S)-5-(6-Chloro-5-((tetrahydrofuran-3-yl)amino)pyrazolo[1,5-a]pyrimidin-3-yl)-N-(methyl- $d_3$ )nicotinamide (**50a**). A mixture of (S)-3-bromo-6-chloro-N-(tetrahydrofuran-3-yl)pyrazolo[1,5-a]pyrimidin-5-amine (50 mg, 0.16 mmol), N-(methyl- $d_3$ )-5-(4,4,5,5-tetramethyl-1,3,2-dioxaborolan-2-yl)nicotinamide (50 mg, 0.19 mmol), Pd(dppf)Cl<sub>2</sub>·CH<sub>2</sub>Cl<sub>2</sub> (13 mg, 16  $\mu$ mol), and sodium carbonate (60 mg, 0.6 mmol) in 1,4-dioxane (1.5 mL) and water (0.5 mL) was sparged with N<sub>2</sub> and heated to 100 °C for 2 h. The reaction mixture was adsorbed onto silica gel directly. The product was purified by flash chromatography (0–100% EtOAc/hexanes followed by 0–20% MeOH/DCM) to afford the title compound (15 mg, 25%). LCMS calculated for  $C_{17}H_{13}D_3ClN_6O_2$  ( $M + H$ )<sup>+</sup>:  $m/z$  = 376.1; found: 376.2.

**Step 7.** (S)-5-(6-(1-Isopropyl-1H-pyrazol-3-yl)-5-((tetrahydrofuran-3-yl)amino)pyrazolo[1,5-a]pyrimidin-3-yl)-N-(methyl- $d_3$ )-nicotinamide (**30**). A mixture of (S)-5-(6-chloro-5-((tetrahydrofuran-3-yl)amino)pyrazolo[1,5-a]pyrimidin-3-yl)-N-(methyl- $d_3$ )-nicotinamide (15 mg, 40  $\mu$ mol), 1-isopropyl-3-(4,4,5,5-tetramethyl-1,3,2-dioxaborolan-2-yl)-1H-pyrazole (28.3 mg, 0.12 mmol), XPhos Pd G2 (1.6 mg, 2.0  $\mu$ mol), and cesium carbonate (39 mg, 0.1 mmol) in 1,4-dioxane (1 mL) and water (0.5 mL) was sparged with N<sub>2</sub> and heated to 100 °C for 2 h. The reaction was diluted with MeOH and filtered through a thiol SiliaPrep cartridge. The product was purified by prep HPLC (pH 2) to afford the title compound (2 mg, 11%). LCMS calculated for  $C_{23}H_{24}D_3N_8O_2$  ( $M + H$ )<sup>+</sup>:  $m/z$  = 450.2; found: 450.2. <sup>1</sup>H NMR (400 MHz, DMSO- $d_6$ )  $\delta$  9.43 (d,  $J$  = 2.1 Hz, 1H), 9.38 (d,  $J$  = 5.8 Hz, 1H), 9.31 (s, 1H), 8.99 (t,  $J$  = 2.2 Hz, 1H), 8.76 (d,  $J$  = 2.0 Hz, 1H), 8.63 (s, 1H), 8.62 (s, 1H), 7.98 (d,  $J$  = 2.4 Hz, 1H), 7.08 (d,  $J$  = 2.5 Hz, 1H), 4.81–4.72 (m, 1H), 4.63 (p,  $J$  = 6.7 Hz, 1H), 4.14 (dd,  $J$  = 9.2, 5.5 Hz, 1H), 3.94 (q,  $J$  = 7.7 Hz, 1H), 3.88 (dt,  $J$  = 8.5, 4.2 Hz, 1H), 3.83 (dd,  $J$  = 9.3, 3.1 Hz, 1H), 2.49–2.43 (m, 1H), 2.05–1.95 (m, 1H), 1.50 (d,  $J$  = 6.6 Hz, 6H).

## ■ ASSOCIATED CONTENT

### SI Supporting Information

The Supporting Information is available free of charge at <https://pubs.acs.org/doi/10.1021/acs.jmedchem.2c01366>.

Full synthetic procedures and characterization of compounds **5–30**; copies of NMR spectra and HPLC traces for compounds **25**, **27**, **29**, and **30**; protocols for all biological assays, pharmacokinetic, and pharmacodynamic studies; and coordinates and experimental details for the X-ray co-crystal structure of **30** (PDF)

Docking models for compound **9** (Figure 2a) (PDB)

Theoretical THF derivative (Figure 2b) bound to FGFR3 (PDB)

Molecular formula strings and *in vitro* biological data (CSV)

## Accession Codes

PDB ID code for **30** bound to FGFR2 is 8E1X. Authors will release the atomic coordinates upon article publication.

## ■ AUTHOR INFORMATION

### Corresponding Author

Artem Shvartsbart – Prelude Therapeutics, Wilmington, Delaware 19803, United States; [orcid.org/0000-0002-1438-3095](https://orcid.org/0000-0002-1438-3095); Email: [ashvartsbart@preludetx.com](mailto:ashvartsbart@preludetx.com)

### Authors

Jeremy J. Roach – Proteovant Therapeutics, King of Prussia, Pennsylvania 19406, United States

Michael R. Witten – Incyte Corporation, Wilmington, Delaware 19803, United States

Holly Koblish – Ikena Oncology, Boston, Massachusetts 02210, United States

Jennifer J. Harris – Incyte Corporation, Wilmington, Delaware 19803, United States

Maryanne Covington – Incyte Corporation, Wilmington, Delaware 19803, United States

Rodrigo Hess – Incyte Corporation, Wilmington, Delaware 19803, United States

Luping Lin – WuXi AppTec, Philadelphia, Pennsylvania 19112, United States

Michelle Frascella – Incyte Corporation, Wilmington, Delaware 19803, United States

Lisa Truong – Incyte Corporation, Wilmington, Delaware 19803, United States

Lynn Leffet – Incyte Corporation, Wilmington, Delaware 19803, United States

Patricia Conlen – Incyte Corporation, Wilmington, Delaware 19803, United States

Elham Beshad – Proteovant Therapeutics, King of Prussia, Pennsylvania 19406, United States

Ron Klabe – Incyte Corporation, Wilmington, Delaware 19803, United States

Kamna Katiyar – Incyte Corporation, Wilmington, Delaware 19803, United States

Laura Kaldon – Incyte Corporation, Wilmington, Delaware 19803, United States

Ruth Young-Sciame – Incyte Corporation, Wilmington, Delaware 19803, United States

Xin He – Incyte Corporation, Wilmington, Delaware 19803, United States

Susan Petusky – Incyte Corporation, Wilmington, Delaware 19803, United States

Kwang-Jong Chen – Incyte Corporation, Wilmington, Delaware 19803, United States

April Horsey – Incyte Corporation, Wilmington, Delaware 19803, United States

Hsiang-Ting Lei – Incyte Corporation, Wilmington, Delaware 19803, United States

Leslie B. Epling – Incyte Corporation, Wilmington, Delaware 19803, United States

Marc C. Deller – Incyte Corporation, Wilmington, Delaware 19803, United States

Oleg Vechorkin – Incyte Corporation, Wilmington, Delaware 19803, United States

Wenqing Yao – Synnovation Therapeutics, Wilmington, Delaware 19803, United States

Complete contact information is available at:

<https://pubs.acs.org/doi/10.1021/acs.jmedchem.2c01366>

## Author Contributions

The manuscript was prepared with contributions from all authors. All authors have given approval to the final version of

the manuscript. A.S., J.J.R., and M.R.W. designed and synthesized the compounds.

### Funding

Funding was provided by Incyte Research Institute, who employed all authors at the time this research was conducted.

### Notes

The authors declare no competing financial interest.

## ACKNOWLEDGMENTS

The authors thank Scott Leonard, James Hall, and Laurine Galya for NMR analysis; Ravi Jalluri and Onur Atasoylu for molecular modeling; Jim Doughty for purity analysis; Min Li for solubility measurements; Leslie Hall, Karen Gallagher, and Hong Chang for their expert technical assistance; and Eddy W. Yue and Matthew McCamant for proofreading the manuscript.

## ABBREVIATIONS

FGFR, fibroblast growth factor receptor; SAR, structure–activity relationships; PK, pharmacokinetics; PD, pharmacodynamics; CYP, cytochrome P450; ADME, absorption, distribution, metabolism, excretion; HBF, hepatic blood flow; MOE, molecular operating environment; AUC, area under the curve; WT, wild-type; PDGFRB, platelet-derived growth factor receptor  $\beta$ ; FLT3, FMS-like tyrosine kinase 3; TRKA, tropomyosin receptor kinase A; FASSIF, fasted-state simulated intestinal fluid; SGF, simulated gastric fluid

## REFERENCES

- (1) Eswarakumar, V. P.; Lax, I.; Schlessinger, J. Cellular signaling by fibroblast growth factor receptors. *Cytokine Growth Factor Rev.* **2005**, *16*, 139–149.
- (2) di Martino, E.; Tomlinson, D. C.; Williams, S. V.; Knowles, M. A. A place for precision medicine in bladder cancer: targeting the FGFRs. *Future Oncol.* **2016**, *12*, 2243–2263.
- (3) Arai, Y.; Totoki, Y.; Hosoda, F.; Shiota, T.; Hama, N.; Nakamura, H.; Ojima, H.; Furuta, K.; Shimada, K.; Okusaka, T.; Kosuge, T.; Shibata, T. Fibroblast growth factor receptor 2 tyrosine kinase fusions define a unique molecular subtype of cholangiocarcinoma. *Hepatology* **2014**, *59*, 1427–1434.
- (4) Katoh, M. Fibroblast growth factor receptors as treatment targets in clinical oncology. *Nat. Rev. Clin. Oncol.* **2019**, *16*, 105–122.
- (5) Montazeri, K.; Bellmunt, J. Erdafitinib for the treatment of metastatic bladder cancer. *Expert Rev. Clin. Pharmacol.* **2020**, *13*, 1–6.
- (6) Perera, T. P. S.; Jovcheva, E.; Mevellec, L.; Vialard, J.; De Lange, D.; Verhulst, T.; Paulussen, C.; Van De Ven, K.; King, P.; Freyne, E.; Rees, D. C.; Squires, M.; Saxty, G.; Page, M.; Murray, C. W.; Gilissen, R.; Ward, G.; Thompson, N. T.; Newell, D. R.; Cheng, N.; Xie, L.; Yang, J.; Platero, S. J.; Karkera, J. D.; Moy, C.; Angibaud, P.; Laquerre, S.; Lorenzi, M. V. Discovery and pharmacological characterization of JNJ-42756493 (Erdafitinib), a functionally selective small-molecule FGFR family inhibitor. *Mol. Cancer Ther.* **2017**, *16*, 1010–1020.
- (7) Roubal, K.; Myint, Z. W.; Kolesar, J. M. Erdafitinib: A novel therapy for FGFR-mutated urothelial cancer. *Am. J. Health Syst. Pharm.* **2020**, *77*, 346–351.
- (8) Liu, P. C. C.; Koblisch, H.; Wu, L.; Bowman, K.; Diamond, S.; DiMatteo, D.; Zhang, Y.; Hansbury, M.; Rupar, M.; Wen, X.; Collier, P.; Feldman, P.; Klabe, R.; Burke, K. A.; Soloviev, M.; Gardiner, C.; He, X.; Volgina, A.; Covington, M.; Ruggeri, B.; Wynn, R.; Burn, T. C.; Scherle, P.; Yeleswaram, S.; Yao, W.; Huber, R.; Hollis, G. INCB054828 (Pemigatinib), a potent and selective inhibitor of fibroblast growth factor receptors 1, 2, and 3, displays activity against genetically defined tumor models. *PLoS One* **2020**, *15*, No. e0231877.
- (9) Merz, V.; Zecchetto, C.; Melisi, D. Pemigatinib, a potent inhibitor of FGFRs for the treatment of cholangiocarcinoma. *Future Oncol.* **2021**, *17*, 389–402.
- (10) Javle, M.; Roychowdhury, S.; Kelley, R. K.; Sadeghi, S.; Macarulla, T.; Weiss, K. H.; Waldschmidt, D. T.; Goyal, L.; Borbath, I.; El-Khoueiry, A.; Borad, M. J.; Yong, W. P.; Philip, P. A.; Bitzer, M.; Tanasanvimon, S.; Li, A.; Pande, A.; Soifer, H. S.; Shepherd, S. P.; Moran, S.; Zhu, A. X.; Bekaii-Saab, T. S.; Abou-Alfa, G. K. Infigratinib (BGJ398) in previously treated patients with advanced or metastatic cholangiocarcinoma with FGFR2 fusions or rearrangements: mature results from a multicentre, open-label, single-arm, phase 2 study. *Lancet Gastroenterol. Hepatol.* **2021**, *6*, 803–815.
- (11) Han, X.; Yang, J.; Li, L.; Huang, J.; King, G.; Quarles, L. D. Conditional deletion of FGFR1 in the proximal and distal tubule identifies distinct roles in phosphate and calcium transport. *PLoS One* **2016**, *11*, No. e0147845.
- (12) Wu, A. L.; Feng, B.; Chen, M. Z.; Kolumam, G.; Zavala-Solorio, J.; Wyatt, S. K.; Gandham, V. D.; Carano, R. A.; Sonoda, J. Antibody-mediated activation of FGFR1 induces FGF23 production and hypophosphatemia. *PLoS One* **2013**, *8*, No. e57322.
- (13) Goyal, L.; Saha, S. K.; Liu, L. Y.; Siravegna, G.; Leshchiner, I.; Ahronian, L. G.; Lennerz, J. K.; Vu, P.; Deshpande, V.; Kambadakone, A.; Mussolin, B.; Reyes, S.; Henderson, L.; Sun, J. E.; Van Seventer, E. E.; Gurski, J. M., Jr.; Baltschukat, S.; Schacher-Engstler, B.; Barys, L.; Stamm, C.; Furet, P.; Ryan, D. P.; Stone, J. R.; Iafrate, A. J.; Getz, G.; Porta, D. G.; Tiedt, R.; Bardelli, A.; Juric, D.; Corcoran, R. B.; Bardeesy, N.; Zhu, A. X. Polyclonal secondary FGFR2 mutations drive acquired resistance to FGFR inhibition in patients with FGFR2 fusion-positive cholangiocarcinoma. *Cancer Discovery* **2017**, *7*, 252–263.
- (14) Goyal, L.; Shi, L.; Liu, L. Y.; Fece de la Cruz, F.; Lennerz, J. K.; Raghavan, S.; Leshchiner, I.; Elagina, L.; Siravegna, G.; Ng, R. W. S.; Vu, P.; Patra, K. C.; Saha, S. K.; Uppot, R. N.; Arellano, R.; Reyes, S.; Sagara, T.; Otsuki, S.; Nadres, B.; Shahzade, H. A.; Dey-Guha, I.; Fetter, I. J.; Baiev, I.; Van Seventer, E. E.; Murphy, J. E.; Ferrone, C. R.; Tanabe, K. K.; Deshpande, V.; Harding, J. J.; Yaeger, R.; Kelley, R. K.; Bardelli, A.; Iafrate, A. J.; Hahn, W. C.; Benes, C. H.; Ting, D. T.; Hirai, H.; Getz, G.; Juric, D.; Zhu, A. X.; Corcoran, R. B.; Bardeesy, N. TAS-120 overcomes resistance to ATP-competitive FGFR inhibitors in patients with FGFR2 fusion-positive intrahepatic cholangiocarcinoma. *Cancer Discovery* **2019**, *9*, 1064–1079.
- (15) Huang, Z.; Chen, H.; Blais, S.; Neubert, T. A.; Li, X.; Mohammadi, M. Structural mimicry of a-loop tyrosine phosphorylation by a pathogenic FGF receptor 3 mutation. *Structure* **2013**, *21*, 1889–1896.
- (16) Kumar, S.; Sharma, R.; Roychowdhury, A. Modulation of cytochrome-P450 inhibition (CYP) in drug discovery: a medicinal chemistry perspective. *Curr. Med. Chem.* **2012**, *19*, 3605–3621.
- (17) Pirali, T.; Serafini, M.; Cargnin, S.; Genazzani, A. A. Applications of deuterium in medicinal chemistry. *J. Med. Chem.* **2019**, *62*, 5276–5297.
- (18) Grossman, H. B.; Wedemeyer, G.; Ren, L. UM-UC-1 and UM-UC-2: characterization of two new human transitional cell carcinoma lines. *J. Urol.* **1984**, *132*, 834–837.
- (19) Sabichi, A.; Keyhani, A.; Tanaka, N.; Delacerda, J.; Lee, I. L.; Zou, C.; Zhou, J. H.; Benedict, W. F.; Grossman, H. B. Characterization of a panel of cell lines derived from urothelial neoplasms: genetic alterations, growth in vivo and the relationship of adenoviral mediated gene transfer to coxsackie adenovirus receptor expression. *J. Urol.* **2006**, *175*, 1133–1137.
- (20) Blom, K. F.; Glass, B.; Sparks, R.; Combs, A. P. Preparative LC-MS purification: improved compound-specific method optimization. *J. Comb. Chem.* **2004**, *6*, 874–883.